Pulsed-Laser–Induced Reactive Quenching at a Liquid-Solid Interface: Aqueous Oxidation of Iron

P. P. Patil, D. M. Phase, S. A. Kulkarni, S. V. Ghaisas, S. K. Kulkarni, S. M. Kanetkar, and S. B. Ogale
Department of Physics, University of Poona, Pune 411 007, Maharashtra, India

and

V. G. Bhide
School of Energy Studies, University of Poona, Pune 411 007, Maharashtra, India
(Received 14 March 1986; revised manuscript received 14 October 1986)

High-power pulsed-laser–induced reactive quenching at a liquid-solid interface is used for the first time to synthesize a metastable form of iron oxide. The oxide phase is characterized by use of the techniques of conversion-electron Mössbauer spectroscopy, Rutherford backscattering spectrometry, x-ray diffraction, and x-ray photoelectron spectroscopy.

PACS numbers: 68.35.Fx, 64.60.My, 76.80.+y, 81.40.Gh

In recent years considerable interest has grown in the use of high-power lasers for processing of material surfaces, by employment of both the thermal and photochemical aspects.[1-6] Pulsed lasers are of particular interest in this regard in view of their highly nonequilibrium processing character, which allows synthesis of novel phases of materials. In most of the experiments on laser-material interactions the main emphasis has been laid on the use of material systems in the solid state and hardly any attempts have been made to explore the possibilities of synthesizing new materials by pulsed-laser–induced reactions in liquid media and at liquid-solid interfaces. Work has been reported in the literature on laser-induced changes in chemical etching rates of solids in liquid media[7-10]; however, such studies employ laser power primarily to activate the surface-mediated physico-chemical processes and do not involve massive energy transfer to the interface leading to interesting synthesis possibilities. In this Letter we report the results of our experiments performed specifically to explore the latter concept. To our knowledge this is the first study of its kind to be reported in the literature.

In the work presented here we have studied the influence of high-power Q-switched ruby laser pulses (30-ns pulse width) on the interface between iron and water. This system is useful as a vehicle to promote the basic idea because the ruby radiation ($\lambda = 0.694$ μm) is transmitted by water and absorbed by iron, leading to major energy deposition into the interface region. Also, since water can chemically react with iron via aqueous oxidation, this system is capable of revealing the reactive aspect of the quenching process.

The iron foils used in these experiments were obtained from Goodfellow metals and were 99.999% pure. These foils were appropriately microetched prior to use. Four characterization techniques, viz. conversion-electron Mössbauer spectroscopy (CEMS),[11-13] Rutherford backscattering spectrometry (RBS), x-ray diffraction (in normal-incidence as well as glancing-angle geometries), and x-ray photoelectron spectroscopy (XPS), were used to study the samples. The Mössbauer spectra were recorded by use of a ^{57}Co:Rh source. The glancing-angle x-ray patterns were obtained on a Rigaku (Japan) machine by keeping the glancing angle of incidence fixed at $\sim 6°$. XPS results were obtained on a VG Mark-IV system.

The specifications of different samples studied are as follows: sample No. 1, virgin iron foil; samples No. 2 and No. 3, iron foils treated with laser pulses underwater at energy densities of 10 and 15 J/cm^2, respectively; sample No. 4, iron foil treated with laser pulses in air at an energy density of 10 J/cm^2. In order to enhance the effects, each spot was irradiated twice.

The CEMS results for samples Nos. 1–4 are shown in Figs. 1(a)–1(d), respectively. In analysis of the CEMS data it must be remembered that each CEMS spectrum represents the state of the sample over a depth of ~ 0.25 μm below the surface. The RBS results for samples No. 1 and No. 2 are given in Fig. 2 and these help reveal the modifications occurring over a depth of ~ 1 μm. The x-ray diffraction data for samples No. 2 and No. 4, which are of interest from the standpoint of comparison between laser treatment in liquid and air ambients, are given in Fig. 3. The corresponding XPS results are presented in Fig. 4.

The CEMS spectrum of Fig. 1(a) shows a single sextet contribution which corresponds to α-Fe (internal magnetic field = 330 kOe), while the spectrum of Fig. 1(b) shows two significant quadrupole-split doublets in addition to α-Fe. One of the doublets has an isomer shift (IS) of 0.85 mm/s and a quadrupole splitting (QS) of 0.64 mm/s; while the other doublet has an IS of 1.09 mm/s and a QS of 0.65 mm/s. The two doublets together correspond to the FeO phase, the IS values being somewhat higher than the values reported for this phase by Elias and Linnett.[14] The gradation of composition over the 0.25-μm depth scanned by the CEMS technique could be responsible for such differences. As the RBS

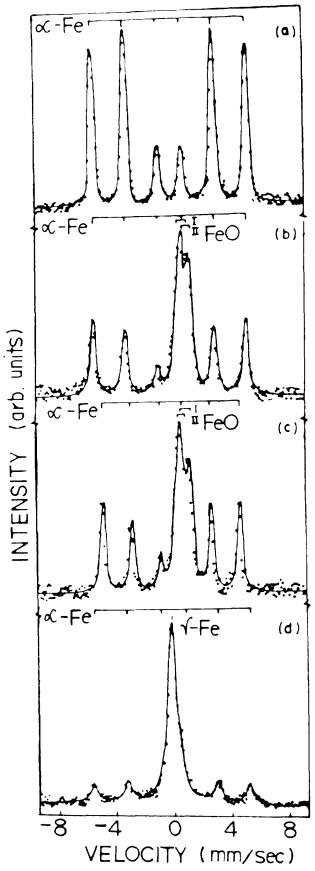

FIG. 1. Room-temperature CEMS spectra of (a) virgin iron foil; (b) iron foil laser treated in H_2O at an energy density of 10 J/cm^2; (c) iron foil laser treated in H_2O at an energy density of 15 J/cm^2; (d) iron foil laser treated in air at an energy density of 10 J/cm^2.

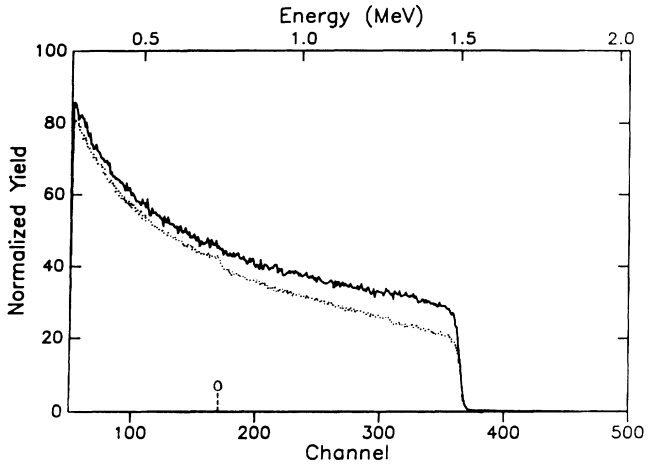

FIG. 2. Rutherford-backscattering spectra of virgin iron foil (dashed line) and iron foil laser treated in H_2O at an energy density of 10 J/cm^2 (dotted line). The spectra were recorded by use of a 2-MeV He^+ beam.

results would indicate, such gradation does exist in the sample. FeO is the most unusual form among the oxides of iron and it can be obtained only by rapid quenching from high temperature.[15] Its presence in our sample brings out the quenching character of the studied process, while its formation from the iron-water system demonstrates the reactive aspect. In order to further justify the formation of this form of iron oxide, we now discuss the RBS, XRD, and XPS data.

The RBS spectra of Fig. 2 reveal that the iron signal is significantly depleted over a depth of ~ 1 μm in the case of sample No. 2 as compared to the case of sample No. 1, the depletion being due to the incorporation of oxygen. Since oxygen has considerably lower values of Z and M as compared to iron, its backscattering cross section is also lower by almost a factor of 10, and hence the corresponding signal is weaker. However, the fact that a small but clear step is seen at the location of the oxygen surface signal (marked "O") shows that a significant quantity of oxygen is incorporated over large depth. On the basis of the computer simulations, the oxygen-incorporated region of sample No. 2 can be roughly divided into three subregions: (i) a top ~ 1000-Å layer having an oxygen concentration of ~ 50 at.%; (ii) an intermediate thick layer (thickness ~ 4500 Å) having a slowly decaying oxygen concentration with an average composition of 40–45 at.%; and (iii) an underlayer having a thickness of ~ 4000 Å over which the oxygen concentration gradually decays to zero. The RBS result thus supports the CEMS observation of near-stoichiometric FeO in the top layer of sample No. 2. As may be noticed, the RBS data also give us information about the oxygen-deficient thick layer in the deeper region, which is inaccessible to the CEMS technique.

The glancing-angle x-ray data given in Fig. 3(a) also show the presence of FeO in the surface layer (~ 1000 Å thick) and this can be further confirmed from the XPS results shown in Figs. 4(a) and 4(c). The XPS depth profiles show that the concentrations of Fe and O are almost comparable to each other in the top 1000-Å layer and in the thick region below the top layer the concentration is uniformly lower, which is consistent with the RBS data. The chemical state of iron and oxygen can be inferred from the "Fe $2p$" and "O $1s$" contributions seen for different depths subsequent to Ar ion sputtering of the overlayers. The positions of these contributions in all oxides of iron have been studied in great detail by Mills and Sullivan[16]; and they point out that the appearance of a satellite peak at an energy of ~ 5 eV above the Fe $2p_{3/2}$ peak is the distinguishing feature of the FeO phase and is absent in the case of other oxides such as Fe_3O_4 and Fe_2O_3. Our spectra clearly show the presence of such a satellite in addition to other aspects discussed by

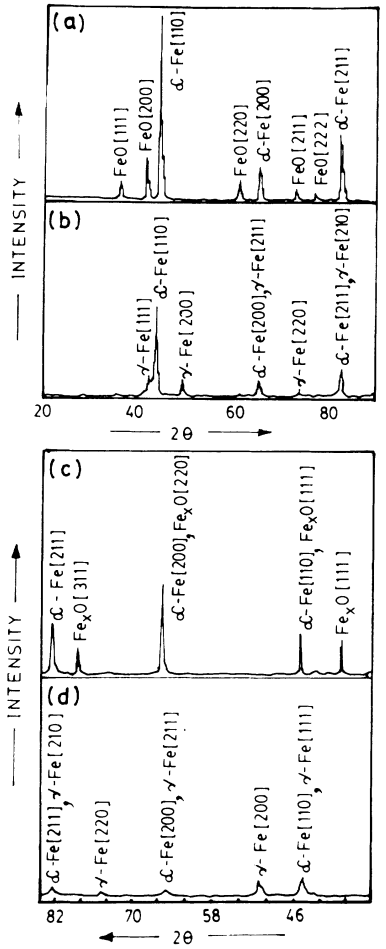

FIG. 3. X-ray diffraction patterns for (a),(c) an iron foil laser treated in H_2O and (b),(d) an iron foil laser treated in air. The energy density in both cases is 10 J/cm^2. The patterns in (a) and (b) are recorded in glancing-angle geometry, while (c) and (d) are recorded in normal-incidence geometry.

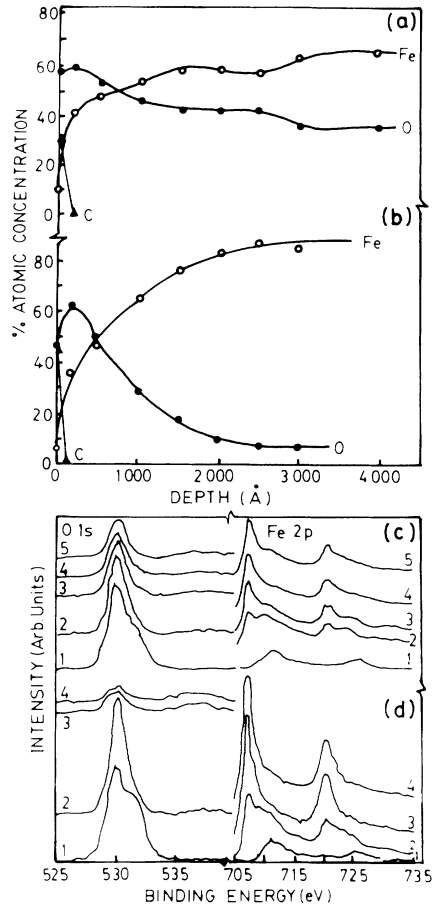

FIG. 4. X-ray photoelectron spectroscopy (XPS) results for (a),(c) an iron foil treated in H_2O and (b),(d) an iron foil laser treated in air. The Fe 2p and O 1s contributions represented by curves 1, 2, 3, 4, and 5 correspond respectively to chemical states at depths of 0, 500, 2000, 3000, and 4000 Å below the surface.

Mills and Sullivan in the context of the FeO phase. This proves beyond doubt that we have an FeO phase in the top surface layer. The O 1s features in the case of the FeO phase have also been discussed by Mills and Sullivan and our results are in good agreement with these as well. The Fe 2p and O 1s contributions indicated by lines 3, 4, and 5 in Fig. 4(c) represent the chemical state of the oxygen-deficient Fe-O coordination, seen in the RBS and XPS depth profiles.

The x-ray diffraction pattern for sample No. 2 obtained in normal-incidence geometry [Fig. 3(c)] allows us to explore further the features of the oxygen-deficient Fe-O coordination mentioned above, since in this geometry the x rays penetrate deeper. The positions of diffraction lines in Fig. 3(c) can be explained by the assumption that contributions of α-Fe and an oxygen-deficient FeO-like coordination having a lattice constant of 4.03 Å coexist in the region explored. On the basis of Vegard's law, applied to α-Fe (lattice constant 2.86 Å) and near-stoichiometric FeO (lattice constant 4.3 Å), one can easily obtain the composition of oxygen-deficient Fe-O coordination to be $\sim Fe_{55}O_{45}$, which is reasonably consistent with the RBS result.

In order to see whether an increase in the laser energy density has a significant influence on the stoichiometry and the basic pattern of observations, we irradiated an iron sample under water at an energy density of 15 J/cm^2. The corresponding CEMS spectrum [Fig. 1(c)] has features similar to those of the spectrum of sample No. 2 [Fig. 1(b)], the IS (QS) values of the doublets being 0.74 (0.72 mm/s) and 1.06 mm/s (0.82 mm/s), which are closer to the values reported by Elias and Lin-

nette.[14] Since an enchanced energy density is expected to enhance the overall process time scale, it could lead to better stoichiometry.

Finally, it is useful to bring out the differences in the results of processing in liquid and in air, by comparison of the states of samples No. 2 and No. 4. Surprisingly, the air-treated sample (No. 4) shows a significant contribution of γ-Fe phase[17] (singlet with an IS of -0.001 mm/s) in addition to a small contribution of FeO-like phase and a contribution due to α-Fe. The presence of γ-Fe can also be inferred from the x-ray diffraction results of Figs. 3(b) and 3(d). The XPS results for sample 4 [Figs. 4(b) and 4(d)] show that the major quantity of the oxygen incorporated in this sample exists in the surface region up to a depth of ~ 600 Å and in the thick underlying region only a dilute concentration of oxygen exists. This oxygen could be responsible for stabilizing the γ-Fe phase, which is not known to be stable in pure form at room temperature except in the form of epitaxial films on fcc substrates.[17] It may be noted that FeO is itself a fcc structure and its formation in distributed regions could help the growth of the fcc phase of iron. The issue of stability of γ-Fe is yet to be fully understood and its presence in our sample remains an interesting subject to be explored further. Nevertheless, our results presented here clearly demonstrate that processing in liquid and air ambients lead to characteristically different results.

We believe that three mechanisms could play an important role in the reactive quenching process reported here: (i) thermodynamic evaporation and chemical reactions at high pressure and temperature; (ii) redeposition of reaction products via rapid rerandomization of atomic trajectories due to the presence of high local pressure; and (iii) convective motions in fluid state being set in by instabilities rendered by high concentration and temperature gradients. The relative contributions of these mechanisms would vary depending upon the laser energy density and pulse duration, properties and reactivities of participating materials, etc. We do not expect that boiling, leading to significant cavitation, would occur at least during the early stages of reaction kinetics because of intrinsic difficulties which may be encountered in satisfying the nucleation requirements. Berti *et al.*[18] have discussed these and related issues in their paper on pulsed-ruby-laser treatment of silicon in gaseous environments at different pressures. Considerable work is required to be done before a reasonable degree of understanding regarding the processes involved can be reached.

This work was supported by the Department of Atomic Energy and the Department of Science and Technology (Goverment of India). Two of us (P.P.P. and S.K.K.) acknowledge financial assistance by the Council for Scientific and Insustrial Research and the Department of Science and Technology (Government of India), respectively. The authors acknowledge fruitful discussions with Dr. S. K. Date, Dr. A. S. Nigavekar, and Dr. V. N. Kulkarni. One of the authors (S.B.O.) gratefully acknowledges useful discussions with Dr. F. W. Saris, FOM-Instituut, The Netherlands. Thanks are also due to Dr. T. Venkatesan (Bell Communications Research, Inc.) for help in obtaining RBS results.

[1]*Laser and Electron Beam Solid Interactions and Material Processing*, edited by J. F. Gibbons, L. D. Hess, and T. W. Sigmon, Materials Research Society Symposium Proceedings Vol. 1 (North-Holland, New York, 1981).

[2]See, for example, the proceedings of a series of conferences on "Energy Beam-Solid Interactions and Transient Thermal Processing" published by North-Holland.

[3]*Laser Processing and Diagnostics,* edited by D. Bauerle (Springler-Verlag, Berlin, 1984).

[4]M. Mayo, Solid State Technol. **29**, 141 (1986).

[5]J. Narayan, R. T. Young, R. F. Wood, and W. H. Christie, Appl. Phys. Lett. **33**, 338 (1978).

[6]E. Fogarassy, R. Stuck, J. J. Grob, and P. Siffert, J. Appl. Phys. **52**, 1076 (1981).

[7]F. A. Houle, Proc. SPIE Int. Soc. Opt. Eng. **459**, 110 (1984).

[8]G. L. Laper and M. D. Tabat, J. Appl. Phys. **58**, 3649 (1985).

[9]S. Mottet and L. Henry, J. Phys. (Paris), Colloq. **44**, C5-139 (1983).

[10]R. M. Osgood, Jr., J. Phys. (Paris), Colloq. **44**, C5-133 (1983).

[11]B. D. Sawicka and J. A. Sawicki, in *Mössbauer Spectroscopy-II,* edited by U. Gonser (Springer, Berlin, 1981).

[12]V. P. Godbole, S. M. Chandhari, S. V. Ghaisas, S. M. Kanetkar, S. B. Ogale, and V. G. Bhide, Phys. Rev. B **31**, 5703 (1985).

[13]S. B. Ogale, Rekha Joshee, V. P. Godbole, S. M. Kanetkar, and V. G. Bhide, J. Appl. Phys. **57**, 2915 (1985).

[14]D. J. Elias and J. W. Linnett, Trans. Faraday Soc. **65**, 2673 (1969).

[15]N. N. Greenwood and T. C. Gibbs, Mössbauer Spectroscopy (Chapman and Hall Ltd., London, 1971), p. 248.

[16]P. Mills and J. L. Sullivan, J. Phys. D **16**, 723 (1983).

[17]U. Gonser and M. Ron, in *Applications of Mössbauer Spectroscopy,* edited by R. L. Cohen (Academic, New York, 1980), Vol. 2, pp. 282–324.

[18]M. Berti, L. F. Dona dalle Rose, A. V. Drigo, C. Cohen, J. Siejka, G. G. Bentini, and E. Jannitti, Phys. Rev. B **34**, 2346 (1986).